Nanoscale measurement of the energy distribution of semiconductor surface states

S. Saraf,[1] A. Schwarzman,[1] Y. Dvash,[1] S. Cohen,[2] D. Ritter,[2] and Y. Rosenwaks[1,*]
[1]*School of Electrical Engineering, Department of Physical Electronics, Faculty of Engineering, Tel-Aviv University, Ramat-Aviv 69978, Israel*
[2]*Department of Electrical Engineering, Technion—Israel Institute of Technology, Haifa 32000, Israel*
(Received 25 September 2005; revised manuscript received 21 November 2005; published 31 January 2006)

We report on a method to quantitatively measure the local energy distribution of surface states density within the band gap of semiconductors using Kelvin probe force microscopy. The method is based on measuring the contact potential difference of a cross-sectional *pn* junction; as the tip scans the junction surface, the surface states population changes, thus modifying the measured local surface band bending. The energy distribution is then obtained by fitting the calculated surface potential to the measured contact potential difference. The method is applied to $p^{++}n$ and $n^{++}p$ Si (110) surfaces and $p^{++}n$ InP (110) surfaces measured under different environments. The results are compared to data obtained by theoretical models and other experimental methods.

DOI: 10.1103/PhysRevB.73.035336 PACS number(s): 73.20.At

I. INTRODUCTION

The electronic properties of semiconductor surfaces are determined by the surface states energy distribution, $N_{SS}(E)$, within their bandgap. This distribution is essential in determining the properties of semiconductor junctions,[1] the phenomenon of Fermi level pinning, surface recombination, and passivation,[2,3] molecules adsorption,[4] leakage current in metal-oxide-semiconductor (MOS) transistors,[5] and more. In addition, the importance of contacts in molecular electronics,[6] suggests that semiconductor electrodes may play an important role,[7] thus the knowledge of the surface states distribution is crucial in determining the charge transfer processes and the current in such devices.

Widely used methods to measure the surface states energy distribution are photoemission spectroscopy (PES) and angle-resolved PES.[8] Interface states energy distribution is measured using capacitance-voltage (*C*-*V*) method,[9] where the capacitance of a metal-insulator-semiconductor (MIS) structure is measured as a function of metal bias. The *C*-*V* method requires a top contact, thus measuring of bare surfaces (i.e., surface versus interface states) is impossible. L. Kronik *et al.* have suggested a contactless method to measure the energy distribution of surface states using surface photovoltage spectroscopy (SPS) with a tunable laser as the excitation source.[10,11]

In recent years the knowledge of the surface states energy distribution and density is crucial in order to accurately quantify two-dimensional carrier profiling with high spatial resolution using scanning capacitance microscopy (SCM)[12,13] and scanning spreading resistance microscopy (SSRM).[14] When the surface states concentration approaches the area dopant concentration at the surface, the measured capacitance and/or resistance is governed by the charged surface states rather than the dopant concentration. In addition, the physics and performance of mesoscopic and nanoscale devices are largely affected by surface states, so their accurate determination with high spatial resolution is necessary.

All the above methods (and others not mentioned here) share a common drawback: they have low spatial resolution. Scanning tunneling microscopy (STM) has been widely used in the last decade to measure local density of surface states,[15] but it requires sufficiently high tunneling currents.

We present here a contactless method, based on Kelvin probe force microscopy (KPFM), to measure surface states energy distribution with high lateral resolution and with very high sensitivity ($\geqslant 1\times 10^{9}$ cm^{-2} eV^{-1}), applicable to semiconductors with a wide range of electrical conductivity. We apply the method to abundant semiconductors (whose surface properties are of great importance) such as oxidized Si (110) surface, and InP (110) cleaved under nitrogen and ultra-high vacuum (UHV) conditions, and discuss the KPFM method and the surface states distributions in comparison to data obtained by other methods.

II. MEASURING THE LOCAL SURFACE STATES DISTRIBUTION USING KPFM

The surface states energy distribution can be obtained by measuring the local band bending as the Fermi level position relative to one of the bands is changed. This is similar to *C*-*V* measurements where the change in interface trap charge density is measured as the surface band bending is varied. The change in the Fermi level position may be achieved by one of the following ways: temperature change, external bias, and change in doping concentration.

The method used in the present work is based on measuring the contact potential difference (CPD) of a cross-sectional *pn* junction using KPFM as shown schematically in Fig. 1. As the tip scans the junction surface, the surface states population changes, thus changing the local surface band bending measured by the KPFM. The surface states energy distribution is then obtained by equating the position derivative of the surface and the space charge region (SCR) charges (Q_{SS} and Q_{SC}, respectively) as shown in detail below.

The total surface charge is given by the following well-known expression:

 ©2006 The American Physical Society

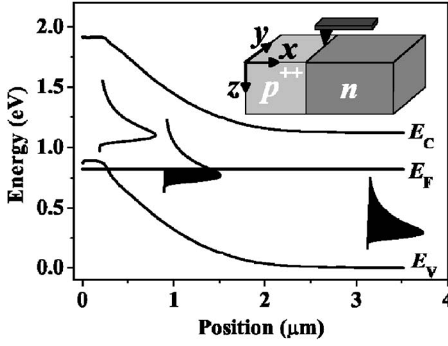

FIG. 1. Schematic description of the surface states energy distribution measurement using KPFM. As the tip scans the junction surface (inset), the surface states population changes, and the resulting change in local band bending is measured by the KPFM.

$$Q_{SS}=q\left(N_t^D\int_{-\infty}^{\infty}N_{SS}^D(E_t)[1-f(E_t,V)]dE_t - N_t^A\int_{-\infty}^{\infty}N_{SS}^A(E_t)f(E_t,V)dE_t\right), \quad (1)$$

where $N_{SS}^{D}(N_{SS}^{A})$ is the donor (acceptor) states energy distribution, $N_t^{D}(N_t^{A})$ is the donor (acceptor) surface states density, E_t is the state energy relative to the valence band maximum, E_V (defined as zero potential energy), when the bands are flat, and q is the electron charge.

The Fermi-Dirac distribution function $f(E_t,V)$ is given by

$$f(E_t,V)=\frac{1}{1+\exp\left(\dfrac{E_t-E_f-qV_S+qV_{junc}}{kT}\right)}, \quad (2)$$

where E_F denotes the Fermi level, V_S is the surface band bending, V_{junc} is the potential in the bulk relative to its value at the low-doped side of the junction, T is the temperature, and k is the Boltzmann constant. Since the surface state occupation changes as the tip scans along the x direction, we calculate the derivative of Eq. (1) with respect to position, x, as

$$\frac{dQ_{SS}}{dx}=q\left[N_t^D\int_{-\infty}^{\infty}N_{SS}^D(E_t)\left(-\frac{df}{dx}\right)dE_t - N_t^A\int_{-\infty}^{\infty}N_{SS}^A(E_t)\frac{df}{dx}dE_t\right]. \quad (3)$$

After inserting the expression for df/dx in Eq. (3) and rearranging terms we obtain

$$\frac{dQ_{SS}}{dx}=\frac{q}{V_t}\left(\frac{dV_{junc}}{dx}-\frac{dV_S}{dx}\right)\times\left[N_t^D\int_{-\infty}^{\infty}N_{SS}^D(E_t)S\left(\frac{E_t-E_F-qV_S+qV_{junc}}{kT}\right)dE_t + N_t^A\int_{-\infty}^{\infty}N_{SS}^A(E_t)S\left(\frac{E_t-E_F-qV_S+qV_{junc}}{kT}\right)dE_t\right], \quad (4)$$

where V_t is the thermal voltage and S is defined by

$$S\left(\frac{E_t-E_F-qV_S+qV_{junc}}{kT}\right)=\frac{\exp\left(\dfrac{E_t-E_F-qV_S+qV_{junc}}{kT}\right)}{\left[1+\exp\left(\dfrac{E_t-E_F-qV_S+qV_{junc}}{kT}\right)\right]^2}. \quad (5)$$

When the full width at half maximum (FWHM) of S is much narrower relative to that of $N_{SS}(E)$, it can be approximated by the Dirac δ function and the integrals in Eq. (4) can be solved analytically to give

$$\frac{dQ_{SS}}{dx}=\frac{qkT}{V_t}\cdot\left(\frac{dV_{junc}}{dx}-\frac{dV_S}{dx}\right)[N_t^DN_{SS}^D(E)+N_t^AN_{SS}^A(E)], \quad (6)$$

where $E\equiv E_F+qV_S-qV_{junc}$.

The surface states energy distribution is then obtained by equating the surface and SCR charge position derivatives:

$$\frac{dQ_{SS}}{dx}=-\frac{dQ_{SC}}{dx}. \quad (7)$$

By using Eq. (6) and rearranging terms, the total surface states energy distribution is obtained in the form

$$N_t^DN_{SS}^D(E)+N_t^AN_{SS}^A(E)=\frac{-\dfrac{dQ_{SC}}{dx}}{\dfrac{qkT}{V_t}\left(\dfrac{dV_{junc}}{dx}-\dfrac{dV_S}{dx}\right)}. \quad (8)$$

V_S and Q_{SC} (and their position derivatives) are extracted from fitting the calculated surface potential to the measured CPD, and V_{junc} is obtained from calculating the bulk built-in potential based on the doping concentration [measured by secondary ion mass spectroscopy (SIMS)]. Calculating $N_{SS}(E)$ using Eq. (8) is done in two steps. In the first step, $N_{SS}(E)$ is found by using Q_{SC} as a fitting parameter to fit the calculated surface potential to the measured CPD, but since the calculation is not self-consistent,[16] an additional iteration is performed in which the initial $N_{SS}(E)$ is used to fit the calculated surface potential to the measured CPD self-consistently, and the final $N_{SS}(E)$ is obtained by using Q_{SC}, calculated in the second step. The other values appearing in Eq. (8) are found as discussed above.

The surface charge, Q_{SS}, state energy, E_t, and the surface band bending, V_S, are interrelated through the Fermi-Dirac distribution function [Eq. (2)], therefore a key factor in the above derivation is the knowledge of V_S at each point on the surface.[17] Figure 2(a) shows the calculated 2D potential distribution of a symmetric Si *pn* junction [dopant concentration of 1×10^{17} cm^{-3} with a density of 1×10^{12} cm^{-2} (5×10^{12} cm^{-2}) of donor (acceptor) type states located at energy of 0.7 eV(0.8 eV) above E_V]. The lower junction built-in potential on the surface, V_{bi}^{S}, compared with the built-in potential in the bulk, V_{bi}^{b}, shown at the "back" of the figure, is due to charged surface states; surface states trap

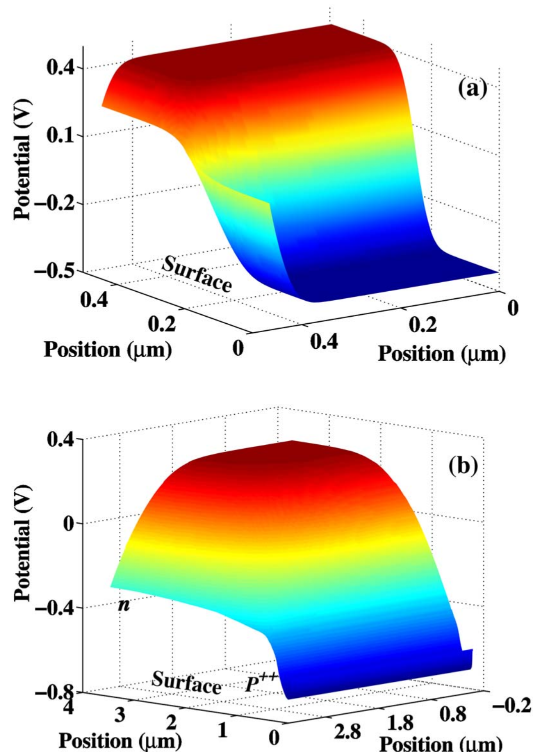

FIG. 2. (Color online) Calculated 2D potential distribution of (a) a symmetric Si *pn* junction and (b) a $p^{++}n$ Si junction showing the effect of the doping concentration on the surface band bending. Zero band bending is observed on the degenerate part of the junction [front right side in (b)].

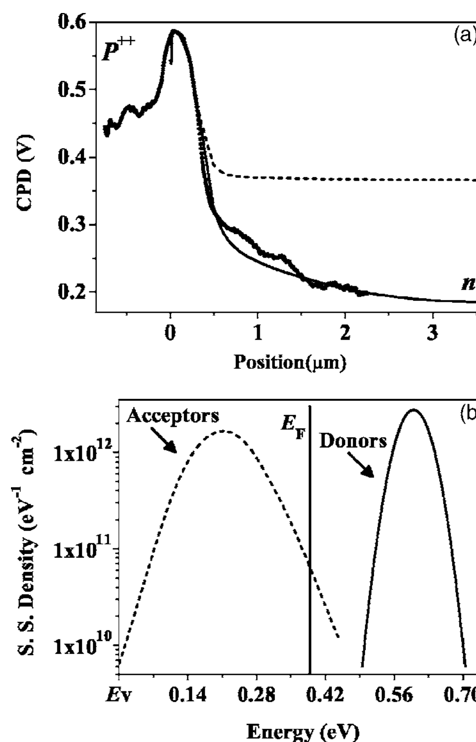

FIG. 3. (a) CPD measured under nitrogen environment (●) and initially calculated (dashed line) surface potential of a $p^{++}n$ Si junction; the solid line is a best fit based on the modified distribution. See text for details. (b) Complete surface states distribution of the low-doped side of the junction, obtained from the fit (solid line) in (a). The acceptor part of the distribution was initially obtained using Eq. (8).

holes (electrons) on the cleaved surface of the $p(n)$ side of the junction, creating depletion-type band bending opposite in sign on each side of the junction. Thus the bands will bend up (down) in the $n(p)$ doped region, with the net result being a reduction of $V_{bi}{}^{S}$ (relative to $V_{bi}{}^{b}$). In the case of an asymmetric diode shown in Fig. 2(b) [with a density of 7.7×10^{11} cm^{-2}(3.2×10^{12} cm^{-2}) of donor (acceptor) type states located at energy of 0.6 eV(0.336 eV) above E_V], the degenerate side of the junction serves as a potential reference since the band bending on this side is negligible. V_S is then determined as the difference between the calculated bulk potential and the (simulated and fitted to the measured CPD) surface potential, calculated from a 2D numerical solution of Poisson and Laplace equations for a semiconductor-vacuum system.

The KPFM measurements were conducted using two different systems: (a) a commercial atomic force microscope (Autoprobe CP, Veeco, Inc.) operating in the noncontact mode (based on a setup described previously[18]) inside a home-built Nitrogen containing glove box (<2 ppm relative humidity) and (b) ultra-high vacuum (UHV) AFM (VT AFM, Omicron Inc.) operated at $p\leqslant10^{-10}$ mbar. In this system the KPFM is measured in the AM mode at the second cantilever resonance frequency as was described in detail in the past.[19]

III. RESULTS

A. Si (110) surface

The surface states distribution of a polished and oxidized $p^{++}n$ Si junction (110) (p-type B-doped implant with a maximum dopant concentration of $\sim1.75\times10^{20}$ cm^{-3} on an n-type As-doped substrate with a dopant concentration of $\sim2.9\times10^{14}$ cm^{-3}), obtained according to the procedure described above, is shown by the dashed line in Fig. 3(b). This distribution is then used to calculate the surface potential; the result is shown by the dashed line in Fig. 3(a). The large difference relative to the measured (under Nitrogen environment) CPD profile is because the energy interval for which $N_{SS}(E)$ is obtained is less than the band gap as will be explained in some detail below. In order to obtain the distribution in a wider energy range, we use an iterative process in which we add another Gaussian distribution of the form $N_{SS}(E)=N_t\exp\{-0.5[(E-E_0)/\sigma]^2\}$ (where N_t is the surface states density at the peak energy, E_0, σ is related to the curve width, and all energies are relative to E_V) to the surface states distribution already obtained, and calculate the surface potential until a good fit like the one shown by the solid line in Fig. 3(a) is obtained; the distribution shown in Fig. 3(b) by the solid line is the part of $N_{SS}(E)$ resulting from this iterative procedure.

The assignment of the surface states type (donor or acceptor) is based on the following argument. Since the low-doped n side of the junction has a depletion-type band bending (due to the lower surface built-in voltage relative to the bulk), it is most likely due to negative surface charge resulting from acceptor-type states located below the surface Fermi level ($\sim$0.39 eV above E_V). However, as shown above, calculating the surface potential using the initially obtained surface states distribution [dashed line in Fig. 3(b)] resulted in a lower built-in surface voltage relative to the measured CPD due to an excess negative surface charge. Therefore a Gaussian distribution of donor-type surface states located above the Fermi level (contributing a positive charge) was required in order to fit the measured CPD. The final distribution, shown in Fig. 3(b), is composed of acceptor states (dashed line) with a peak density of 1.65×10^{12} cm^{-2} at energy of 0.21 eV above E_V, and donor states (solid line) with a peak density of 2.77×10^{12} cm^{-2} at energy of 0.6 eV and FWHM of 0.07 eV.

It is important to compare the surface states distribution obtained here for the oxidized Si (110) with previously reported data. Flietner[20] has reported on several calculated surface states distributions at the Si/SiO_2 interface: the P_L and P_H distributions of extrinsic donor-type states with FWHM of 0.12 and 0.08 eV located 0.4 and 0.7 eV above E_V, respectively, and the U_M distribution extending over most the band gap, with a lower (upper) donor (acceptor)-type intrinsic states. Apart from the states type of the low-energy peak of U_M, this is in very good agreement with our result; the low-energy peak of U_M is located 0.2 eV above E_V with a density of $\sim2.5\times10^{12}$ cm^{-2} eV^{-1} and the P_H peak is located 0.7 eV above E_V with a density of $\sim1\times10^{12}$ cm^{-2} eV^{-1}. Füssel *et al.*[21] have attributed the U_M, P_L, and P_H distributions to dangling bond defect centers of the character $Si_{3-x}O_x$-Si. Poindexter *et al.* have also reported on interface states peaks located at similar bandgap energies.[22] The well-known U shape distribution resulting from intrinsic surface states with donor (acceptor)-type states located at the lower (upper) half of the band gap cannot be observed in our measurements, because the energy interval of the obtained distribution is less than the energy gap (see the discussion below).

Figure 4(a) shows the measured CPD (symbols) and calculated (solid line) surface potential of a $n^{++}p$ Si diode (110) (n-type As-doped implanted buried layer with a maximum dopant concentration of $\sim5.45\times10^{19}$ cm^{-3} on a p-type B-doped substrate with a dopant concentration of $\sim3\times10^{15}$ cm^{-3}) cleaved and immersed in a 10% HF solution for a period of 15 min prior to measurement under nitrogen environment. The final distribution, shown in Fig. 4(b), is composed of an approximately rectangular donor states (dashed line) distribution with a peak density of $\sim5.28\times10^{11}$ cm^{-2} at an energy of $\sim$0.94 eV above E_V and a Gaussian distribution of acceptor states (solid line) with a peak density of 1×10^{10} cm^{-2} at an energy of 0.4 eV and FWHM of $\sim$0.12 eV. Comparing our results to the calculation of Flietner[20] shows (as in the case of the $p^{++}n$ junction) agreement with the P_L distribution (peak energy location and FWHM) and the upper peak of the U_M distribution located $\sim$0.9 eV above E_V with a peak density of $\sim1.2\times10^{12}$ cm^{-2}.

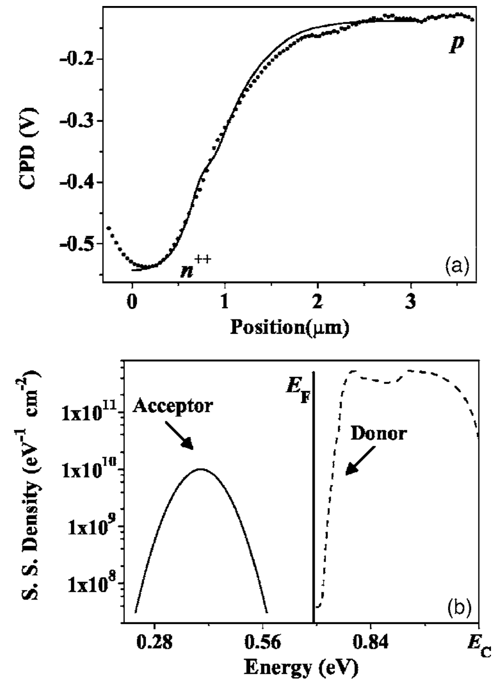

FIG. 4. (a) CPD measured under nitrogen environment (●) and calculated (solid line) surface potential of a $n^{++}p$ Si junction. (b) Complete surface states distribution of the low-doped side of the junction, obtained from the fit (solid line) in (a).

B. InP (110) surface

Figure 5(a) shows the measured CPD (symbols) and calculated surface potential (solid line) of a $p^{++}n$ InP junction cleaved under nitrogen environment, and the measured CPD of the same structure cleaved inside UHV. The InP sample was grown by a compact metalorganic molecular beam epitaxy similar to the system described before.[23] Beryllium served as the p-type dopant with a dopant concentration of $\sim4.5\times10^{18}$ cm^{-3}, and the n-type layer was Sn doped with a dopant concentration of $\sim5.3\times10^{15}$ cm^{-3}. Figure 5(b) shows the complete surface states energy distribution of the InP surface measured under nitrogen environment, obtained by fitting the result of the direct calculation (symbols) using Gaussian distributions. The acceptor-type distribution (solid line) is a sum of two Gaussian curves with $N_t=2.47\times10^{12}$ cm^{-2}, $E_0=0.586$ eV, and $\sigma=0.086$ eV ($\sigma=0.028$ eV) for the lower (upper) part of the distribution. The donor part of the distribution (dashed line) is a Gaussian curve with $N_t=3.8\times10^{12}$ cm^{-2}, $E_0=0.615$ eV, and $\sigma=0.014$ eV. Figure 5(c) shows the surface states energy distribution obtained from the direct calculation [Eq. (8)] for the InP sample cleaved and measured inside UHV. The lower (upper) part of the distribution is an acceptor (donor)-type states with $N_t=6.12\times10^{11}$ cm^{-2} ($N_t=8.1\times10^{11}$ cm^{-2}) at energy of 0.21 eV(0.68 eV) and the so-called charge neutrality level is located at $\sim$0.51 eV. The main differences relative to the results obtained under nitrogen environment are the peak

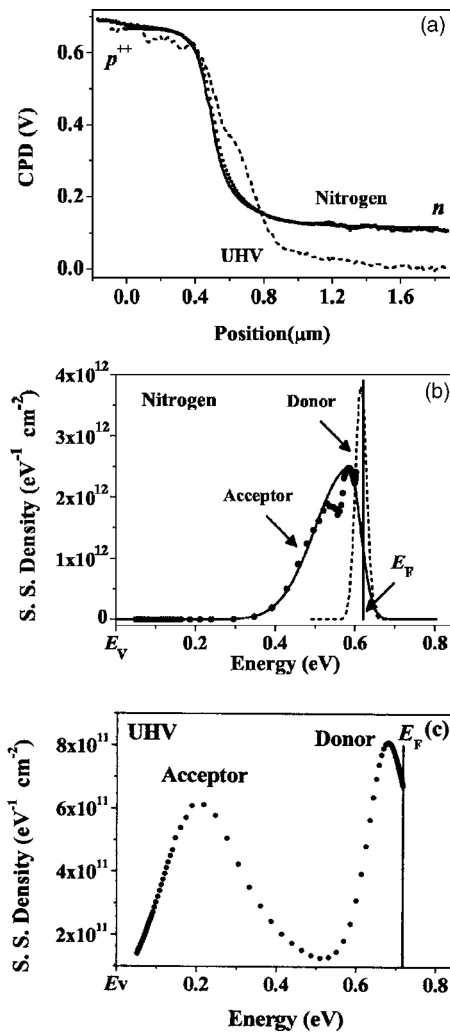

FIG. 5. (a) Measured CPD (●) and calculated surface potential (solid line) of a $p^{++}n$ InP junction cleaved under nitrogen environment, and the measured CPD of the same structure cleaved inside UHV (dashed line). (b) Complete surface states distribution of the low-doped side of the InP sample cleaved and measured under nitrogen environment. (c) Surface states energy distribution of the low-doped side of the InP sample cleaved and measured inside UHV.

energy location (peak density) of the acceptor type states, 0.586 eV(2.47×10^{12} cm^{-2}) vs. 0.21 eV(6.12×10^{11} cm^{-2}) for the InP measured under nitrogen and UHV distributions, respectively. On the other hand, the donor-type states distribution peaks are located at similar energies, 0.615 and 0.68 eV for the glove box and UHV distributions, respectively. This similarity indicates that adding another peak to the distribution obtained from the direct calculation in order to fit the surface potential (the donor part of the glove box distribution [dashed line of Fig. 5(b)]) enables us to extend the states distribution energy interval and obtain similar results to the direct calculation (the donor part of the UHV distribution [upper peak of the distribution in Fig. 5(c)]), which is unambiguously determined by Eq. (8). The differences between the two donor distributions (width and peak density) may result from the approximation made in solving

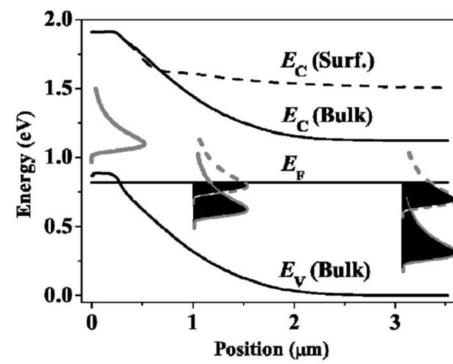

FIG. 6. Calculated bulk (solid line) and surface (dashed line) band structure of a $p^{++}n$ Si junction (the surface valence band is omitted for clarity). An arbitrary surface states distribution inside the band gap is shown for three different positions as the tip scans the junction surface, showing the reduced measured energy interval (denoted as black filled area under the distribution curves) of the surface states distribution (dashed line) compared to the case of negligible band bending (solid line).

the integrals of Eq. (4) as explained below, therefore these parameters are not taken into account in the comparison.

Previously reported data on surface states energy distribution of InP surfaces show some agreement with our results. Shapira *et al.*[24] reported on a single surface state located at 0.2 eV for n-InP (110) sample cleaved and measured under UHV. Burstein *et al.*[25] obtained the same result for an undoped InP (100) sample and attributed it to residual impurities. These results (state type and energy location), obtained by SPS measurements, are in excellent agreement with the low-energy peak of the UHV distribution (0.2 eV). Ahaitouf *et al.*[26] reported on a continuous state distribution at the upper half of the band gap of a (100) n-InP with a peak density of 4.5×10^{12} cm^{-2} eV^{-1} located at 0.79 eV, which is 0.11 eV higher than the donor peak energy location of the UHV measured distribution (0.68 eV).

IV. DISCUSSION

Figure 6 shows the calculated bulk (solid line) and surface (dashed line) band structure of a $p^{++}n$ Si structure (the surface valence band is omitted for clarity) with an arbitrary surface states distribution located inside the band gap. Since one side of the junction is low doped and due to the fact that the surface band bending reduces the built in surface potential, only part of the surface states energy distribution is measured. This is illustrated in Fig. 6 by the fact that as the tip moves across the junction, E_F "scans" a wider energy range of the states distribution in the case of small (insignificant in the figure) band bending (solid line) relative to the case of a larger surface band bending (dashed line). Hence, only a part of the distribution (black filled area under the distribution curve) crosses E_F, i.e., from the low-energy end of the distribution up to the intersection with the Fermi level (in the case of a $p^{++}n$ sample); the other part, from the intersection with E_F up to the high-energy end, remains above E_F and therefore is not measured and the result of the analysis based

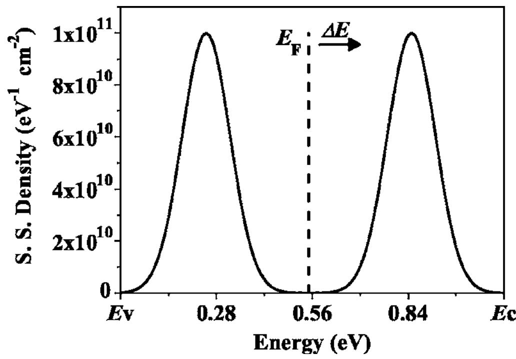

FIG. 7. Schematic description of two arbitrary surface states distributions inside the band gap. Raising the Fermi level by ΔE increases the net negative surface charge regardless of the states type.

on Eq. (8) gives only a portion of the distribution as described in the previous section.

The left-hand side of the expression for the surface states distribution [Eq. (8)] is additive, indicating that the surface states type (i.e., donor or acceptor) cannot be unambiguously distinguished using our method. This is demonstrated in Fig. 7, which shows two Gaussian shape surface states distributions within the band gap, located below and above the Fermi level (dashed line). Two possibilities have to be considered, i.e., the lower (upper) distribution is a donor (acceptor) type or vice versa. In the first case, the donor (acceptor) states are all occupied (empty) and the overall surface charge is approximately zero. Raising the Fermi level energy by ΔE will populate empty acceptor states and increase the overall negative surface charge. In the second case, the donor (acceptor) states are all empty (occupied) and the overall surface charge is again nearly zero. Raising the Fermi level by ΔE would populate empty donor states, reduce the positive surface charge, and increase the overall negative surface charge. Hence, in both cases the total surface charge becomes more negative as the Fermi level energy is raised, which means that our junction scanning method cannot directly distinguish between donor- and acceptor-type surface states in this case, and other considerations have to be taken into account in order to determine the states type (see the discussion above for the $p^{++}n$ Si junction). On the other hand, the nature of a single-type surface states distribution inside the energy gap can be unambiguously determined according to the sign of the surface band bending, i.e., upward (downward) for acceptor- (donor) type surface states for an n-type semiconductor.

The sensitivity of our method is demonstrated by calculating the influence of small changes of the measured CPD (for example ~20 mV) on the obtained $N_{SS}(E)$. Figure 8(a) shows the original and slightly modified surface potentials (solid and dashed lines, respectively) of a $p^{++}n$ Si junction. The original surface potential is a solution of Poisson equation, which is then modified by decreasing the built-in potential. Figure 8(b) shows the surface states distributions correspond to the original and modified surface potentials (solid and dashed lines, respectively); these distributions are obtained from the analysis based on Eq. (8) as described above.

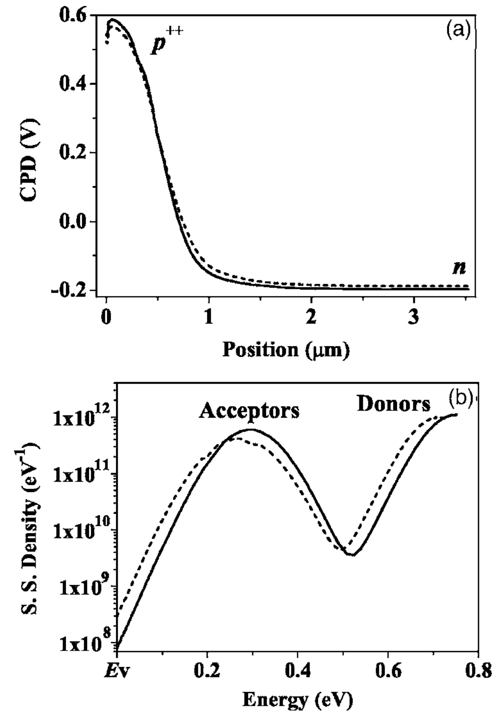

FIG. 8. (a) Calculated (solid line) and intentionally modified (dashed line) surface potential of a $p^{++}n$ Si junction. (b) The corresponding surface states distributions extracted for the two cases demonstrate the sensitivity of our method.

Except from a small shift towards lower energies and minor changes in the surface states density, the distributions obtained from the modified and original surface potentials are almost the same, showing the small effect of noise of the measured CPD on the extracted distribution.

The error in the obtained surface states distribution has several contributions, among them are the measurement noise of the KPFM (typically 5 to 10 mV); the error of the dopant profile measured by SIMS, the truncation error of the numerical calculation of the Poisson solver, the error in the deconvolution of the real CPD images, and the error of approximating the derivative of the Fermi-Dirac function as a Dirac δ function. Some of the errors are doping dependent, for example the error in the calculated surface charge on the degenerate side of the junction is higher relative to the low-doped side. Therefore it is very hard to estimate the error of the obtained distribution and each case should be examined separately; however, the most significant error (in the states density), which increases as the actual distribution is narrower, stems from the approximation of the Fermi-Dirac distribution function as a δ function, which results in a broadened $N_{SS}(E)$ and decreased surface states density in the vicinity of the peak energy relative to the original one. This error can be considerably decreased, by solving the integrals of Eq. (4) using direct numerical algorithms from the field of inverse theory.

In conclusion, we have presented a contactless method to measure the local energy distribution of surface states within the band gap of semiconductors using KPFM with high

sensitivity down to 1×10^9 cm^{-2} eV^{-1}. The method was applied to (110) surface of Si $p^{++}n$ and $n^{++}p$ junctions and the results were in a good agreement with reported theoretical models and experimental results. The results obtained for InP (110) surfaces, measured under nitrogen and UHV environments, were in some agreement with surface states distributions measured by other methods. The energy interval of the obtained distribution was discussed and it was shown that the results are insensitive to small variations of the measured CPD.

ACKNOWLEDGMENTS

The authors acknowledge financial support from Israel Science Foundation (ISF Grant No. 1118/04) and the German Israeli Science Foundation (GIF Grant No. 801/03).

*Electronic address: yossir@eng.tau.ac.il

[1] W. Mönch, *Semiconductor Surfaces and Interfaces* (Springer-Verlag, Berlin, 1993).
[2] Y. Rosenwaks, I. Tsimberova, H. Gero, and M. Molotskii, Phys. Rev. B **68**, 115210 (2003).
[3] R. Williams, J. Phys. Chem. Solids **23**, 1057 (1962).
[4] A. Vilan, A. Shanzer, and D. Cahen, Nature (London) **404**, 166 (2000).
[5] A. A. Asuha, O. Maida, Y. Todokoro, and H. Kobayashi, Appl. Phys. Lett. **80**, 4552 (2002).
[6] A. Nitzan and M. A. Ratner, Science **300**, 1384 (2003).
[7] N. P. Guisinger, M. E. Greene, R. Basu, A. S. Baluch, and M. C. Hersam, Nano Lett. **4**, 55 (2004).
[8] For a comprehensive discussion and examples, see H. Lüth, *Surfaces and Interfaces of Solids* (Springer-Verlag, Berlin, 1993).
[9] E. H. Nicollian and J. R. Brews, *MOS Physics and Technology* (Wiley, New York, 1982).
[10] L. Kronik and Y. Shapira, Surf. Sci. Rep. **37**, 1 (1999).
[11] L. Kronik, L. Burstein, and Y. Shapira, Appl. Phys. Lett. **63**, 60 (1993).
[12] V. V. Zavyalov, J. S. McMurray, and C. C. Williams, J. Appl. Phys. **85**, 7774 (1999).
[13] J. Yang and F. C. Kong, Appl. Phys. Lett. **81**, 4973 (2002).
[14] D. Álvarez, J. Hartwich, M. Fouchier, P. Eyben, and W. Vandervorst, Appl. Phys. Lett. **82**, 1724 (2003).
[15] R. J. Hamers, Annu. Rev. Phys. Chem. **40**, 531 (1989).
[16] Instead of calculating Q_{SC} resulting from a specific surface states distribution, it is used as a boundary condition for the potential calculation.
[17] S. Saraf and Y. Rosenwaks, Surf. Sci. Lett. **574**, L35 (2005).
[18] R. Shikler, T. Meoded, N. Fried, and Y. Rosenwaks, Appl. Phys. Lett. **74**, 2972 (1999).
[19] Y. Rosenwaks, R. Shikler, T. Glatzel, and S. Sadewasser, Phys. Rev. B **70**, 085320 (2004).
[20] H. Flietner, Surf. Sci. **200**, 463 (1988).
[21] W. Füssel, M. Schmidt, H. Angermann, G. Mende, and H. Flietner, Nucl. Instrum. Methods Phys. Res. A **377**, 177 (1996).
[22] E. H. Poindexter, G. J. Gerardi, M. E. Rueckel, P. J. Caplan, N. M. Johnson, and D. K. Biegelsen, J. Appl. Phys. **56**, 2844 (1984).
[23] R. A. Hamm, D. Ritter, and H. Temkin, J. Vac. Sci. Technol. A **12**, 2790 (1994).
[24] Y. Shapira, L. J. Brillson, and A. Heller, Phys. Rev. B **29**, 6824 (1984).
[25] L. Burstein and Y. Shapira, Semicond. Sci. Technol. **8**, 1724 (1993).
[26] A. Ahaitouf, A. Bath, E. Losson, and E. Abarkan, Mater. Sci. Eng., B **52**, 208 (1998).